

Little-Parks like oscillations in lightly doped cuprate superconductors

Menghan Liao¹, Yuying Zhu², Shuxu Hu¹, Ruidan Zhong³, John Schneeloch^{3,4}, Genda Gu³, Ding Zhang^{1,2,5,6*}, and Qi-Kun Xue^{1,2,5,7*}

¹ *State Key Laboratory of Low Dimensional Quantum Physics and Department of Physics, Tsinghua University, Beijing 100084, China*

² *Beijing Academy of Quantum Information Sciences, Beijing 100193, China*

³ *Condensed Matter Physics and Materials Science Department, Brookhaven National Laboratory, Upton, New York 11973, USA*

⁴ *Department of Physics and Astronomy, Stony Brook University, Stony Brook, New York 11794, USA*

⁵ *Frontier Science Center for Quantum Information, Beijing 100084, China*

⁶ *RIKEN Center for Emergent Matter Science (CEMS), Wako, Saitama 351-0198, Japan*

⁷ *Southern University of Science and Technology, Shenzhen 518055, China*

*Corresponding author.

Email: dingzhang@mail.tsinghua.edu.cn, gqxue@mail.tsinghua.edu.cn

Abstract

Understanding the rich and competing electronic orders in cuprate superconductors may provide important insight into the mechanism of high-temperature superconductivity. Here, by measuring $\text{Bi}_2\text{Sr}_2\text{CaCu}_2\text{O}_{8+x}$ in the extremely underdoped regime, we obtain evidence for a distinct type of ordering, which manifests itself as resistance oscillations at low magnetic fields (≤ 10 T) and at temperatures around the superconducting transition. By tuning the doping level p continuously, we reveal that these low-field oscillations occur only when $p < 0.1$. The oscillation amplitude increases with decreasing p but the oscillation period stays almost constant. We show that these low-field oscillations can be well described by assuming a periodic superconducting structure with a mesh size of about 50 nm. Such a charge order, which is distinctly different from the well-established charge density wave and pair density wave, seems to be an unexpected piece of the puzzle on the correlated physics in cuprates.

A fundamental property of superconductivity is the fluxoid quantization, which can manifest itself in a superconducting hollow cylinder through a periodically modulated superconducting transition temperature (T_c) as a function of magnetic field—the so-called Little-Parks effect [1,2]. It stems from the modulated kinetic energy of the supercurrent as a joint effect of the discrete jumps in the fluxoid winding number and the continuously increasing external magnetic field. Experimentally, Little and Parks observed oscillations in the magneto-resistance at a fixed temperature close to T_c [1], because a modulated T_c could be directly translated to the oscillating resistance via: $\Delta R = \Delta T_c \times dR/dT$. Lately, such a fundamental type of resistance oscillations has been employed not only for the demonstration of pairing in more exotic situations such as the superconductor-insulator transition regime [3, 4] but also for addressing the unconventional pairing symmetry [5]. In most cases, the material under investigation needs to be nanopatterned into a ring or a periodic network [6-9]. Observing this type of oscillations in superconductors without artificial patterning often suggests highly non-trivial quantum physics at play, such as the presence of chiral edge state in MoTe₂ [10] or a spontaneously emerged periodic order in TiSe₂ [11, 12]. The latter phenomenon was attributed to the periodic domains of commensurate charge density wave (CCDW) separated by incommensurate charge density wave (ICDW). Understanding the charge orders is also of high interest due to their omnipresence among high-temperature cuprate superconductors [13, 14]. So far, charge ordering in cuprates was primarily addressed by sophisticated techniques such as resonant X-ray scattering (RXS) or scanning tunneling microscopy (STM). Here we report evidence for charge ordering, although of a distinct type, in a high temperature superconductor—Bi₂Sr₂CaCu₂O_{8+x} (Bi-2212) through transport measurements. Our work provides a fresh perspective at the interplay between superconductivity and charge ordering in the underdoped regime.

Results

Characterization of lightly doped samples. We investigate transport properties of Bi-2212 over a wide doping range by further optimizing the technique we developed previously [15], which includes fabrication of ultrathin Bi-2212 samples and ionic solid gating. Figure 1a shows one of our samples (S1)—a mechanically exfoliated flake of Bi-2212 (highlighted in blue, about 50 nm thick, 80 × 220 μm² lateral size). By applying positive gate voltages (1 to 2 V) to the backside of the substrate—a solid ion conductor, lithium ions can intercalate into Bi-2212 (inset of Fig. 1a). We gate S1 for a certain period of time (right panels of Fig. 1b) and collect temperature (T) dependent resistances after each step of gating. Figure 1b shows that the normal-state resistance increases and the zero-field superconducting transition temperature T_{c0} drops consecutively,

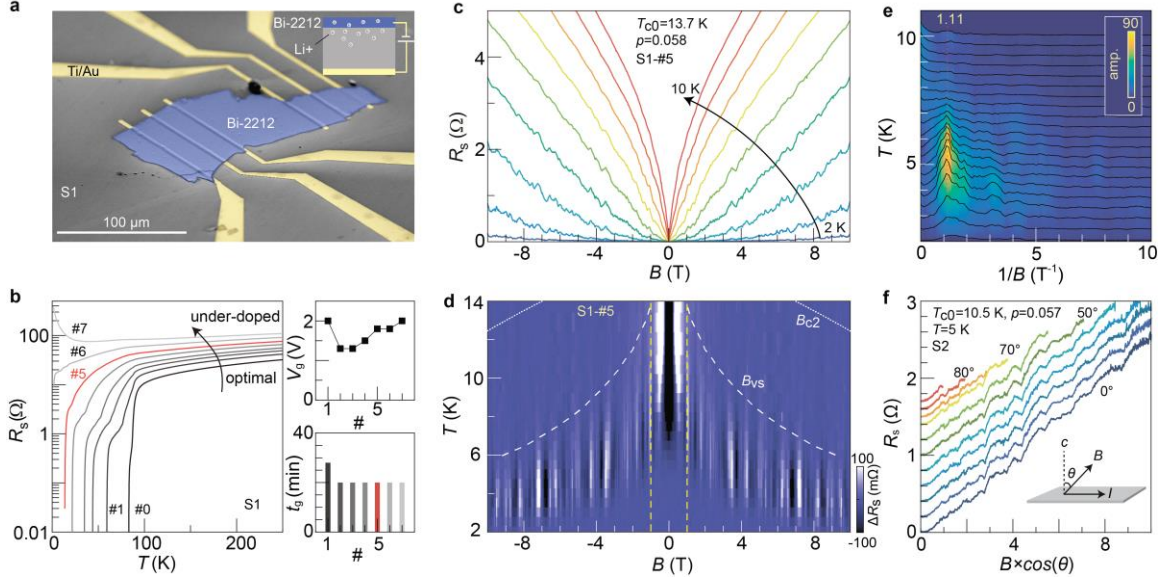


Fig. 1 Resistance oscillations in underdoped Bi-2212. **a**, False-color scanning electron microscopy image of sample S1. The Bi-2212 flake (electrode) is highlighted in blue (yellow). The substrate is a solid ion conductor containing lithium ions. The inset illustrates the gating configuration. **b**, Main panel: temperature dependent resistances of S1 at sequentially gated states. Right panels: gating voltages (V_g) and estimated gating time periods (t_g) for each sequence. t_g includes the complete course of gating at three stages: warming up from 280 K to 300 K; staying at 300 K; cooling down from 300 K to 280 K. V_g is applied throughout the above-mentioned course of time. **c**, Sheet resistance of S1 in an under doped state (S1-#5) as a function of magnetic field at a selected set of temperatures (from 2 to 10 K in steps of 1 K). We estimate the doping level p by using the experimentally measured T_{c0} and the formula: $T_{c0} = T_{c,max}[1 - 82.6(p - 0.16)^2]$. **d**, Color plot of the background subtracted resistance ΔR of S1-#5. Bright and dark stripes in the magnetic range from -1 to 1 T (dashed vertical lines) are artefacts from over-smoothing. Data outside this region is not affected. White dashed curve indicates the line where the resistance reaches 10% of the normal state resistance (zero-field resistance value at 87 K). It represents the phase boundary between the vortex solid (vs) and the vortex liquid. White dotted curve is a guide to the eye, illustrating the expected temperature dependence of the upper critical fields. **e**, Fast Fourier transform (FFT) of the resistance traces at different temperatures in **d**. The dotted line with the number marks the peak position in FFT. **f**, Angular dependent study of the magneto-resistance of S2 as a function of the perpendicular magnetic field. The angle θ is between the total magnetic field and the normal to the sample plane (inset). It increases from 0° to 70° in steps of 10° and from 75° to 85° in steps of 5° . Curves are vertically offset for clarity.

demonstrating the tunability from the nearly optimal doped state ($p = 0.16$) to the extremely underdoped region ($p \sim 0.05$).

At each fixed p , we measure the magneto-resistance. Figure 1c gives exemplary traces of S1 after the fifth gating (S1-#5), corresponding to an under-doped state with $T_{c0}=13.7$ K ($p=0.06$). A finite resistance sets in at a fairly small magnetic field, which reflects the melting of a vortex solid into the liquid phase in high-temperature superconductors [16-19]. In comparison, conventional low-temperature superconductors usually exhibit a clear transition from zero-resistance to finite resistance at the upper critical field— B_{c2} . Despite the complication brought by the vortex liquid phase, we extrapolate the melting field— $B_{vs}(T)$ (demarcated in Fig. 1d as a white curve) to absolute zero to estimate a lower bound of $B_{c2,min}$ [19] (Supplementary Note 1). The superconducting coherence length ξ_0 can be determined via $\xi_0 = \sqrt{\Phi_0/(2\pi B_{c2,min})}$, where $\Phi_0 = h/2e$ is the flux quantum. For S1-#5, we obtain $\xi_0 = 4.6$ nm, in agreement with values obtained for underdoped $\text{YBa}_2\text{Cu}_3\text{O}_{6+x}$ (YBCO) or $\text{Bi}_2\text{Sr}_2\text{CuO}_{6+x}$ (Bi-2201) [18,19]. (The estimated values of ξ_0 at other doping levels are shown in Supplementary Figure 2.) The temperature dependence of $B_{c2}(T)$ is schematically drawn in Fig. 1d by connecting $(B, T) = (0, T_{c0})$ to $(B_{c2,min}, 0)$ as done in ref. [19] with a quadratic curve.

Magneto-resistance oscillations. On top of the increasing trend of the magneto-resistances, we observe regular dips, which occur repeatedly in multiple samples, including a one unit-cell (1-UC) thick Bi-2212 without lithium intercalation (Figs. 1c and 2, Supplementary Figure 3 and 4). Samples were measured in two cryogenic systems and we further excluded possible extrinsic contributions by sweeping the magnetic field with different rates, in different directions, in different cool-downs, and applying different excitation currents (Supplementary Figure 5). Figure 1c shows that the oscillations occur at the same B -field positions symmetrically around $B = 0$ T for different scans at various temperatures. Figure 1d shows data in a finer temperature step, where we subtract each curve with a smoothed background (Supplementary Note 5). Vertical zebra stripes appear below the $B_{vs} - T$ curve. They always occur far below B_{c2} , such that the contribution from the normal state remains minimal. The stripes vanish when Bi-2212 plunges deep into the superconducting state. In Fig. 1e, we carry out fast Fourier transformation (FFT) of the traces at different temperatures by assuming B -periodic oscillations. A sharp peak occurs below 7 K and becomes most prominent at around 5 K, which corresponds to the trace in Fig. 1c (dark green) showing almost linear magneto-resistance. The FFT peak position stays the same— 1.11 T^{-1} (vertical dashed line) at different temperatures. It corresponds to a period in ΔB of 0.9 T.

We further show that the oscillations are of two-dimensional (2D) nature. Here, we measure sample S2 at a similar doping to S1-#5. We employ a setup where the sample can be rotated within an applied magnetic field. The measurement temperature is chosen such that the general behavior of the magneto-resistance is linear, in order to better

appreciate the oscillating features. Figure 1f plots the magnetoresistance of S2 as a function of the perpendicular component of the magnetic field. Clearly, the peaks and dips in traces obtained at different rotation angles occur at the same perpendicular magnetic fields, although the corresponding in-plane magnetic fields are sharply different.

In addition, samples S1 to S4 show multiple superconducting transitions, indicating possible inhomogeneity in doping. However, we observe pronounced resistance oscillations only in the extremely underdoped regime, in which the temperature dependent resistance shows predominantly a single transition. By contrast, in the gated state where the multi-step transition is most pronounced (gated state #1 to #3 of S1, for example), we observe no magneto-resistance oscillations. For sample S5 and S6 shown in the supplementary information (Supplementary Figure 3, 4), under-doping is achieved by natural loss of oxygen. Apart from the superconducting transition at the corresponding T_{c0} of the underdoped situation, a small kink at around 87 K can be identified. However, this kink clearly originates from the nearby regions (thicker flakes, for example) with the initial optimal doping. The underdoped regions in S5 and S6 essentially possess only a single superconducting transition. Still, we observe pronounced resistance oscillations.

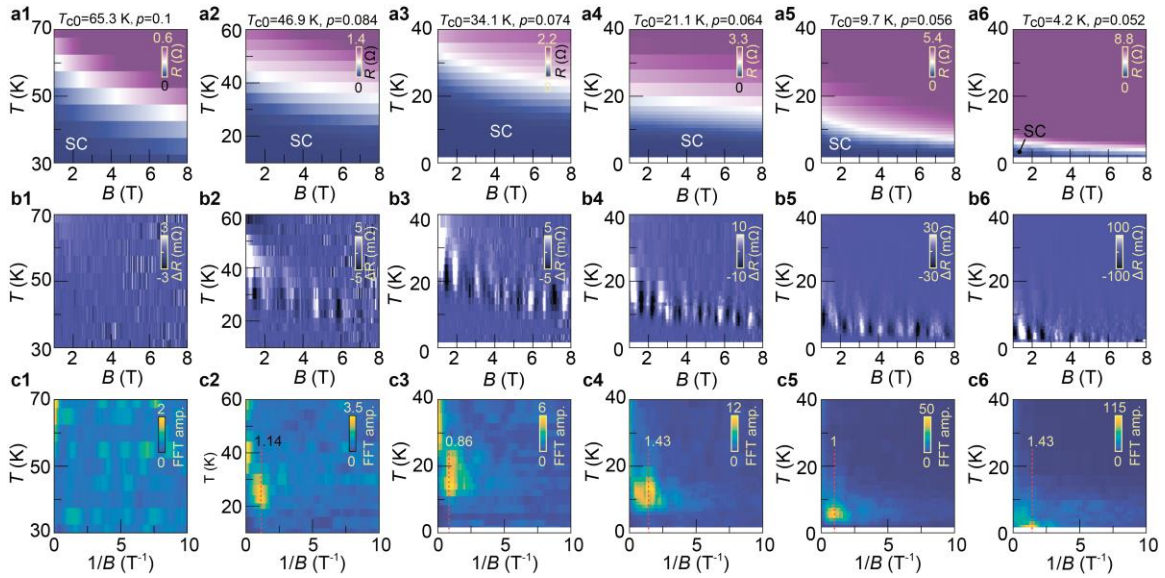


Fig. 2 Doping dependence of the magneto resistance and the oscillations. **a1-a6**, Color-coded resistance of sample S3 as a function of magnetic field and temperature $R(B, T)$. The white stripe demarcates the boundary between the superconducting (SC) region and the normal state. **b1-b6**, Background subtracted resistance as a function of magnetic field and temperature: $\Delta R(B, T)$. The oscillation amplitude increases with decreasing doping. **c1-c6**, FFT of $\Delta R(B)$ at different temperatures. Vertical dotted lines with numbers indicate the peak positions. Each column of this figure corresponds to the same doping level indicated on the top.

The resistance oscillations are therefore not correlated with the apparent multi-step transition.

Doping dependence. Facilitated by our *in-situ* gating techniques, we vary the doping level in a single sample and investigate the evolution of resistance oscillations. Figure 2 shows data sets of sample S3. We select the representative results at 6 doping levels out of the total 10 superconducting states we realized. They are arranged from left to right with decreasing p , which follows the gating sequence. Figure 2a shows the color-coded magneto-resistance. In each panel, the purple areas represent the normal state and the dark blue regions indicate the superconducting regime. The white color corresponds to the resistance value that is half of the normal state resistance, indicating the superconducting transition region. Figure 2b shows the background subtracted data $\Delta R(B, T)$. The zebra stripes are prominent in Fig. 2b2-b6 ($p \leq 0.084$) but are missing in Fig. 2b1 ($p = 0.1$). These stripes always appear in the superconducting transition region (slightly below the white bands in figures of the top row of Fig. 2), reaffirming their intimate link to superconductivity. The oscillation amplitude increases monotonically with

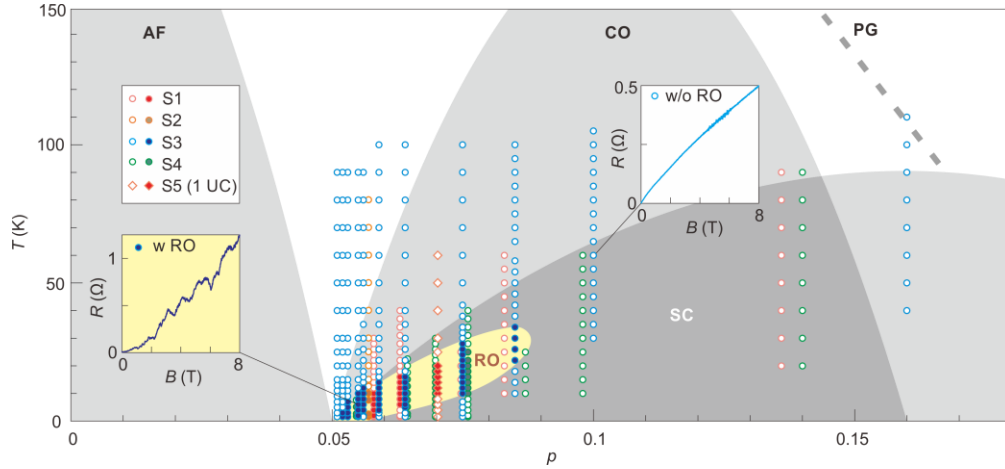


Fig. 3 Phase diagram of the Little-Parks like resistance oscillations in Bi-2212. Each symbol represents a fixed set of temperature and doping at which the magnetoresistance measurement was carried out. Filled (empty) symbols indicate that resistance oscillations—RO—were present (absent). Exemplary traces are shown in the inset boxes. Overlapping data points at $p=0.055$, 0.064 , 0.07 and 0.075 are slightly shifted horizontally for better presentation. In the low temperature regime where resistance oscillations occurred, the actual measurements were taken with denser sets of temperature points (with steps of $\Delta T = 0.5$ K) than represented here ($\Delta T = 2$ K). Gray shadows and dashed curve indicate the typical phases: anti-ferromagnetism (AF), charge order (CO), pseudo-gap (PG), and superconductivity (SC). Here data points marked as S1 and S4 are from the same flake but with two different pairs of contacts in two separate regions. S5 is a 1-UC Bi-2212 flake that is in the underdoped regime after exfoliation. Yellow shadow highlights the region where RO can be experimentally observed.

decreasing doping as indicated by the increasing scales of the color bars. In Fig. 2c, we show the FFT results at different doping levels. The vertical dotted lines mark the peak positions, which seem to show little doping dependence. Their values are consistent with that obtained in sample S1. In Fig. 3, we summarize the experimentally investigated temperature points and doping levels for five samples. We use filled symbols to indicate that resistance oscillations (RO), such as those shown in Fig. 1 c, d, f and Fig. 2b2-b6, are experimentally observed. The filled points cluster in the lightly doped regime ($p \leq 0.08$) of the superconducting dome. It indicates that RO are reproducible across different samples, as long as the samples are tuned into the extremely underdoped regime.

Discussion

First, we exclude quantum oscillations of the normal state as the origin for the observed oscillations. As alluded to before, the resistance oscillations only occur at magnetic fields below the phase boundary between the vortex solid and vortex liquid. These magnetic fields are far below the upper critical field, such that the contribution from the normal state can be neglected. Furthermore, gating our sample into the non-superconducting state (the left-most column of data points in Fig. 3), the resistance oscillations disappear in the experimentally accessible temperature range (down to 1.6 K). It indicates that the resistance oscillations are closely related to the superconducting state.

Studying quantum oscillations in cuprates, instead, often requires the combination of ultrahigh-quality single crystals [typically $\text{YBa}_2\text{Cu}_3\text{O}_{6+x}$ (YBCO) or $\text{Tl}_2\text{Ba}_2\text{CuO}_{6+x}$ (TBCO)] and high magnetic field facilities. The necessity of a powerful magnet is not only because of large upper critical fields in cuprates. It also stems from the criterion for observing quantum oscillations [20, 21]: charge carriers should be able to complete at least one cyclotron orbit before scattering, i.e. $\omega_c \tau \geq 1$, where ω_c is the cyclotron frequency and τ is the scattering time. This requirement can be equivalently expressed by the product of carrier mobility (μ) and magnetic field (in SI units): $\mu B \geq 1$, because $\mu B = e\tau/m^*B = \omega_c \tau$, where m^* is the effective mass. For high quality YBCO and TBCO crystals, μ is on the order of 0.001 to 0.01 $\text{m}^2/\text{V s}$ (10 to 100 $\text{cm}^2/\text{V s}$) [20, 21], allowing the observation of quantum oscillations at $B \sim 50\text{-}100$ T. In comparison, we estimate that the mobility of Bi-2212 is about 1 $\text{cm}^2/\text{V s}$ [15], such that quantum oscillations are expected to occur at $B > 10^4$ T. Any oscillations observed below 10 T cannot stem from quantum oscillations of the normal state.

Second, our results differ from the low- B oscillations of mesoscopic origin as reported previously. Table 1 summarizes the comparison. Resistance oscillations were observed in nanobridges or nanowires of a variety of superconductors [22-25]. They were attributed to the rearrangement of vortex lattice in the bridge/wire or formation of multiply

connected loops [26]. These mesoscopic effects play a major role for samples with a width that is comparable to ξ_0 . By contrast, our sample has a width on the order of tens of micrometers, i.e. $10^5 \xi_0$. The mesoscopic effect should be substantially suppressed in our case. In fact, we find that narrowing the width down to 1 μm neither enhances the resistance oscillations nor changes the period (Supplementary Note 3), further excluding the possible involvement of mesoscopic effects. Recently, anomalous resistance oscillations with pronounced periodicity were reported in various superconducting films [27]. However, the reported oscillations showed isotropic magnetic field dependence, different from the behavior seen in Fig. 1f. Their period is also one order of magnitude smaller.

Apart from resistance oscillations, Nernst effect, which is particularly sensitive to vortex motions, revealed oscillations in Bi-2212 [28]. There, oscillations emerged at the beginning of the rising slope of the Nernst signal, where the vortex solid just started to melt into the liquid phase. It was thus speculated that, around the solid-liquid phase boundary, the vortex lattice may still remain in some regions. Adding new vortices causes plastic deformation such that the Nernst signal fluctuates. At still higher magnetic field—deep in the vortex liquid phase, no more plastic deformation would occur, and the Nernst signal showed a monotonic increase. However, the oscillations caused by the plastic flow of vortices are not expected to occur at the same perpendicular fields with different in-plane magnetic fields, as we observed in Fig. 1f. The energetics of vortices change drastically once an in-plane magnetic field is introduced, because additional Josephson vortices emerge [29]. Additionally, the oscillations in Nernst signal only occurred at

Previous studies		This study
Superconducting nano-bridge [22-25]	Sample width $\sim \xi$	Sample width $\gg \xi$
Superconducting strip [27]	Isotropic	Anisotropic (2D)
	$\Delta B \sim 0.1 \text{ T}$	$\Delta B \sim 1 \text{ T}$
Nernst effect in Bi-2212 [28]	OP-Bi2212: yes UD-Bi2212: no	OP-Bi2212: no UD-Bi2212: yes
Little-Parks oscillations in TiSe_2 [11, 12]	$T \sim 1 \text{ K}, B < 0.6 \text{ T}$	$T \sim 10 \text{ K}$

Table 1 Comparison between the resistance oscillations of this work and the previously reported low-field oscillations in transport.

optimal doping and vanished in the underdoped case. It indicates that the effect of plastic flow of vortices is suppressed in the underdoped regime. By contrast, none of our samples at optimal doping showed oscillations in magneto-resistance. Resistance oscillations only occur deep in the underdoped regime. Therefore, electrical resistance and thermoelectric Nernst measurements probably probe oscillations of different origins.

We now consider the relation between our results and the Little-Parks oscillations. Our results are reminiscent to the intriguing phenomenon recently observed in ionic liquid gated TiSe_2 [11] and lithium intercalated TiSe_2 [12], but at temperature and magnetic field that are both over one order of magnitude higher. In TiSe_2 , it was proposed that a periodic structure emerged: CCDW patches with ICDW stripes at the domain boundaries. At low temperatures, the ICDW regions became superconducting while CCDW regions remain non-superconducting. Cooper pairs going around the superconducting periodic mesh can experience the Little-Parks effect. The superconducting transition temperature oscillates as a function of magnetic field with a period of $\Delta B = \Phi_0/a^2$, where a is the spatial periodicity. At a fixed T close to the unmodulated T_c , the oscillating part of T_c in turn gives rise to resistance oscillations with the same period. In what follows, we assume that a similar periodic structure occurs spontaneously in Bi-2212, as schematically drawn in Fig. 4a. We then test the corresponding theoretical models and discuss the implications. Figure 4a summarizes the extracted periodicity a from all the samples we investigated. The periodic structures are very similar across samples with different thicknesses and sizes, reaffirming an intrinsic origin. It also indicates that this effect is essentially

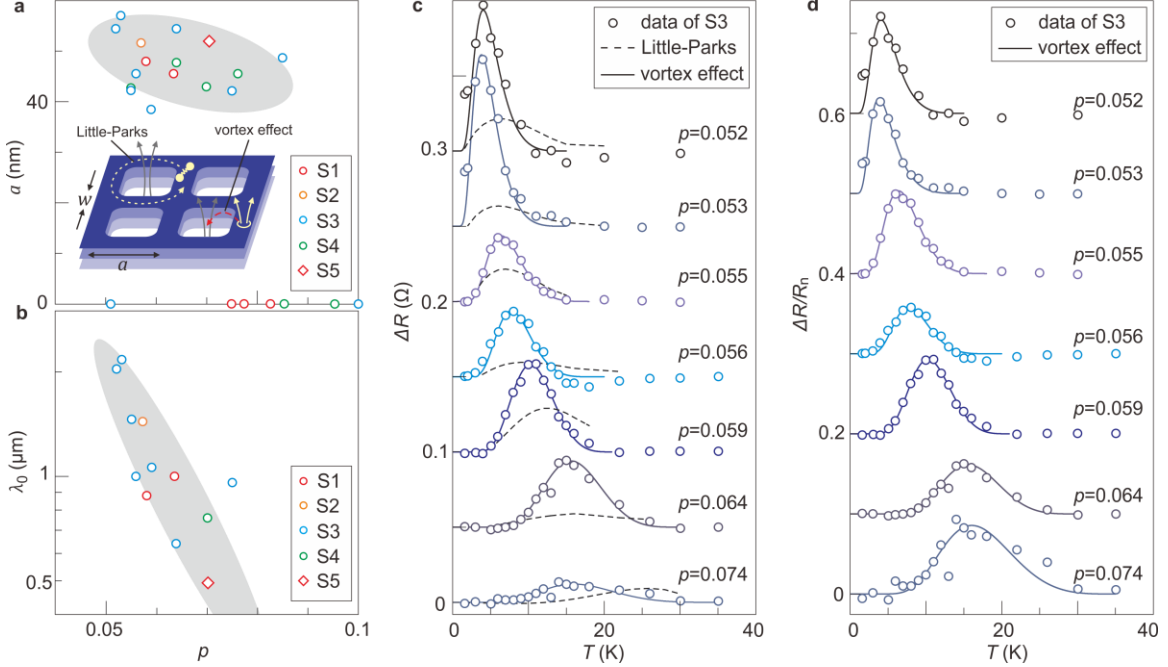


Fig. 4 Quantitative analysis of the Little-Parks like resistance oscillations. **a**, Extracted spatial period as a function of doping for different samples. Inset schematically illustrates the Little-Parks effect and the vortex effect in a periodic superconducting array. The colored mesh indicates the superconducting region. The empty squares indicate the non-superconducting region. **b**, Penetration depth extracted by fitting the temperature dependent oscillation amplitude. **c**, oscillation amplitude as a function of temperature $\Delta R(T)$ at different doping levels for sample S3. They are obtained by calculating the absolute difference between the local and nearest-neighboring maximum and minimum in the $\Delta R(B)$ traces ($B \in [1, 4] T$) at each p and T . Dashed curves are the expected oscillation amplitudes according to the Little-Parks effect. Solid curves are the theoretical fits by taking into account the vortex effect [Eq. (1)]. Data points and curves are vertically offset by 0.05Ω for clarity. **d**, same data sets as shown in **c** but normalized by the normal state resistance R_n . They are vertically offset by 0.1 for clarity.

representative of bulk crystals, although technically thin flakes can be more easily tuned in the doping level.

Apart from the oscillating period, we carry out a quantitative analysis of the oscillating amplitude. At each T and p , we extract ΔR from the difference between the neighboring local minimum and maximum in the resistance trace as a function of B , after subtracting the smoothed background. Figure 4c plots the typical results from sample S3 as a function of T . In comparison, we theoretically estimate the oscillating amplitude expected for the Little-Parks effect. For a square array with a side length of a (Fig. 4a), the Little-Parks effect gives rise to an oscillation depth ΔT_c [30]: $\Delta T_{c,L-P}/T_c = \pi^2/16(\xi_0/a)^2$. The oscillation amplitude in resistance ΔR_{L-P} can be then evaluated via $\Delta R_{L-P} = \Delta T_{c,L-P}(dR/dT)$. By using the experimentally determined ξ_0 , a and dR/dT , we obtain

ΔR_{L-P} as a function of T , which is plotted as dashed curves in Fig. 4c. Clearly, ΔR_{L-P} is much weaker than the experimentally observed oscillations, albeit with similar temperature dependence.

In order to quantitatively describe the resistance oscillations, we have to take into account the vortex effect in a periodic superconducting array. In cuprate superconductors, vortices play a much important role than those in low temperature superconductors do [29]. Thermally excited vortices can cross the superconducting array. This process causes fluxoid transition and modulates T_c in a similar fashion to that of Little-Parks effect (see inset of Fig. 4a). Such a vortex effect was demonstrated to contribute predominantly to the resistance oscillations in periodically patterned $\text{La}_{2-x}\text{Sr}_x\text{CuO}_4$ films [8]. In this scenario, the oscillating amplitude follows the formula [8]:

$$\Delta R = R_n (2E_1/k_B T)^2 \frac{I_1[(E_v + E_1)/2k_B T]}{I_0[(E_v + E_1)/2k_B T]^3}. \quad (1)$$

Here R_n is the normal state resistance, I_0 and I_1 are the zero- and first-order modified Bessel function of the first kind, respectively. The two energy quantities are: $E_1 = \Phi_0^2/8\pi\mu_0\Lambda(T) \cdot w/a$ and $E_v = \Phi_0^2/2\pi\mu_0\Lambda(T) \cdot \ln(2w/\pi\xi(T))$, where μ_0 is the vacuum permeability, w is the separation between the squares (inset of Fig. 4a). $\Lambda(T)$ is the Pearl penetration depth: $2\lambda(T)^2/d$, where d is the superconducting thickness. The temperature dependent penetration depth and coherence length are: $\lambda(T) = \lambda_0/\sqrt{1 - (T/T_c)^2}$, $\xi(T) = 0.74\xi_0/\sqrt{1 - T/T_c}$.

As shown in Fig. 4c and d as solid curves, our data can be nicely fit by Eq. (1). Here we plug in the estimated ξ_0 , a and T_c and use R_n , λ_0 and w as three fitting parameters (Supplementary Note 6 and Supplementary Table 1). Figure 4b and Supplementary Figure 7 summarize the extracted values of λ_0 from different samples. Together, they suggest a clearly increasing trend with decreasing doping. This behavior is understandable, because the superfluid density, which is inversely proportional to the square of the penetration depth, decreases with reduced doping in the underdoped regime. The extracted values of λ also follow the doping dependence extrapolated from previous experimental results on Bi-2212 superconductors [31, 32] (see Supplementary Figure 7). The consistent values and doping dependence suggest that our speculation of a periodic structure captures important physics of the observed phenomenon.

Our results indicate that there exists a distinct phase in the lightly doped cuprate superconductors with large spatial periodicity of about 50 nm (hereafter referred to as P-50). The surprisingly large periodic structure has not been reported before. RXS and STM experiments identified charge ordering (CO) with a small period of about $4a_0$ [13, 14]. As shown in Fig. 3, CO spans in a wide doping range of the phase diagram. By contrast, P-50 here emerges only in the extremely underdoped regime $p \leq 0.08$. Despite the sharp

differences, there could be an intimate link between P-50 and CO, in a similar fashion to those periodic structures observed in TaS₂ [33] and speculated to exist in TiSe₂ [11, 12]. In these transition metal dichalcogenides, CCDW and ICDW phases are identified in the phase diagram as a function of doping or pressure. Individually, CCDW and ICDW have small periods, but a large periodic structure emerges in the regime where they coexist. Around $p = 0.1$, CO is commensurate with a period of $4a_0$. By decreasing p , previous experiments observed a drop in the spatial period by about 15% when p changes from 0.1 to 0.05, suggesting that CO becomes incommensurate [13, 14]. We conjecture that such an evolution may not be uniform spatially. CO with different periods may coexist at $p < 0.1$. If there exist predominantly regions with two periods, for example: $(4 - \delta - \frac{\sigma}{2})a_0$ and $(4 - \delta + \frac{\sigma}{2})a_0$, where $\delta < 0.5$ and $\sigma \ll 0.1$, a large superstructure may appear with a period at around $(4 - \delta)a_0/\sigma$. Here σ only need to be as small as 0.03 to account for the 50-nm period. The weak doping dependence of a (see Fig. 4b) can also be explained. It suggests that with increasing δ at lower p the spread of σ becomes smaller. Although the above scenario remains speculative, a recent finding indeed showed that CDW in cuprates tend to be locally commensurate but globally incommensurate [34], suggesting the coexistence and competition between them.

In summary, we study transport properties of Bi-2212 thin flakes in the underdoped regime and observe peculiar resistance oscillations at low magnetic fields. Samples with different thicknesses and sizes reproducibly show low- B resistance oscillations in the lightly doped regime with consistent oscillating periods. It indicates that there exists a spontaneously emerged periodic structure in the underdoped Bi-2212 ($p \leq 0.08$) with a size of about 50 nm. We speculate that such a large periodic structure may emerge as a competition between the commensurate and incommensurate charge ordering. Our work not only highlights the rich and enticing physics in extremely underdoped high temperature superconductors but also demonstrates a facile technique to access this less-explored regime. Future experimental work may be devoted to unveiling the large periodic structure in real space by scanning probe microscopy.

Methods: Bi-2212 thin flakes were fabricated in a glovebox with Ar atmosphere ($H_2O < 0.1$ ppm, $O_2 < 0.1$ ppm). Mechanical exfoliation was carried out by using standard scotch tape technique. Thin flakes were first exfoliated onto Gel-Films and then dry-transferred onto solid ion conductors or SiO_2/Si substrates [15]. For sample S1, S4, and S5, we pre-patterned electrodes (5nm Ti/30 nm Au) and then placed the Bi-2212 flake on top of the electrodes. For sample S2 and S3, we deposited thin graphite flakes as bottom contacts and then placed BSCCO on top. For the 1UC-Bi-2212 flake, we further capped it with a thin flake of hexagonal boron nitride (hBN) as a protection layer. Samples were then taken out for wire-bonding and subsequent measurements. Silver paste was applied to the backside of the solid ion conductor as the back-gating electrode. The time period for air exposure was kept as short as 20 minutes.

Transport measurements were carried out in two closed-cycle cryogenic systems (Oxford Instruments TelatronPT: 1.55-300 K, 9/12 T) with three different inserts. The electrical resistance was measured in a standard four-terminal configuration by using either the AC lock-in technique (S1, S4, and S5, excitation current: $1 \mu A$) or a combination of DC current source and voltmeter (Keithley 6221 and 2182A) in the delta mode (S2 and S3, excitation current: $10 \mu A$). The DC gate voltage was applied with a source measure unit (Keithley 2400).

Data availability: All data needed to evaluate the conclusions are available in the main text or the supplementary information.

Code availability: The computer code used for data analysis is available upon request from the corresponding author.

Acknowledgments: We thank Hongyi Xie, Haiwen Liu, Yayu Wang, Hong Yao, Fa Wang for fruitful discussions. This work is financially supported by the Ministry of Science and Technology of China (2017YFA0302902, 2017YFA0304600); the National Natural Science Foundation of China (grant No. 51788104, 11790311, 11922409, 12004041) and the Beijing Advanced Innovation Center for Future Chips (ICFC). Work at Brookhaven is supported by the Office of Basic Energy Sciences, Division of Materials Sciences and Engineering, U.S. Department of Energy under Contract No. DE-SC0012704.

Author contributions: M.L., D.Z. and Q.-K. X. initiated the project. M.L., Y.Z. and S.H. fabricated the samples and carried out transport measurements. R. Z., J. S., and G.G grew the single crystals. M.L. and D.Z. analyzed the data and wrote the paper.

Competing interests: Authors declare that they have no competing interests.

References

- [1] W. A. Little, R. D. Parks, Observation of quantum periodicity in the transition temperature of a superconducting cylinder. *Phys. Rev. Lett.* **9**, 9–12 (1962).
- [2] M. Tinkham. Consequences of fluxoid quantization in the transitions of superconducting films. *Rev. Mod. Phys.* **36**, 268 (1964).
- [3] M. D. Stewart Jr., Aijun Yin, J. M. Xu, James M. Valles Jr. Superconducting Pair Correlations in an Amorphous Insulating Nanohoneycomb Film. *Science*, **318**, 1273-1275 (2007).
- [4] C. Yang, et al., Intermediate bosonic metallic state in the superconductor-insulator transition. *Science*, **366**, 1505-1509 (2019).
- [5] Y. Li, X. Xu, M. –H. Lee, M. –W. Chu, C. L. Chien, Observation of half-quantum flux in the unconventional superconductor β -Bi₂Pd. *Science*, **366**, 238-241 (2019).
- [6] B. Pannetier, J. Chaussy, R. Rammal, J. C. Villegier, Experimental fine tuning of frustration: two-dimensional superconducting network in a magnetic field, *Phys. Rev. Lett.* **53**, 1845 (1984).
- [7] P. L. Gammel, P. A. Polakos, C. E. Rice, L. R. Harriott, D. J. Bishop, Little-Parks oscillations of T_c in patterned microstructures of the oxide superconductor YBa₂Cu₃O₇: Experimental limits on fractional-statistics-particle theories, *Phys. Rev. B*, **41**, 2593 (1990).
- [8] I. Sochnikov, A. Shaulov, Y. Yeshurun, G. Logvenov, I. Božović. Large oscillations of the magnetoresistance in naopatterned high- T_c superconducting films. *Nat. Nanotech.* **5**, 516–519 (2010).
- [9] C. G. L. Bøttcher, et al., Superconducting, insulating and anomalous metallic regimes in a gated two-dimensional semiconductor–superconductor array. *Nat. Phys.* **14**, 1138-1144 (2018).
- [10] W. Wang, et al. Evidence for an edge supercurrent in the Weyl superconductor MoTe₂. *Science*, **368**, 534-537 (2020).
- [11] L. J. Li, et al. Controlling many-body states by the electric-field effect in a two-dimensional material. *Nature*, **529**, 185-189 (2016).
- [12] M. Liao, et al. Coexistence of resistance oscillations and the anomalous metal phase in a lithium intercalated TiSe₂ superconductor. *Nat. Commun.* **12**, 5432, (2021).
- [13] R. Comin, A. Damascelli, Resonant X-ray scattering studies of charge order in cuprates. *Annu. Rev. Conden. Matter Phys.* **7**, 369-405 (2016).
- [14] A. Frano, S. Blanco-Canosa, B. Keimer, R. J. Birgeneau. Charge ordering in superconducting copper oxides *J. Phys: Conden. Matter*, **32**, 374005 (2020).
- [15] M. Liao, et al. Superconductor–insulator transitions in exfoliated Bi₂Sr₂CaCu₂O_{8+ δ} flakes. *Nano Lett.* **18**, 5660-5665 (2018).

- [16] Z. A. Xu, N. P. Ong, Y. Wang, T. Kakeshita, S. Uchida, Vortex-like excitations and the onset of superconducting phase fluctuation in underdoped $\text{La}_{2-x}\text{Sr}_x\text{CuO}_4$. *Nature*, **406**, 486-488 (2000).
- [17] Y. Wang, et al. Dependence of upper critical field and pairing strength on doping in cuprates. *Science*, **299**, 86-89 (2003).
- [18] J. Chang, et al. Decrease of upper critical field with underdoping in cuprate superconductors. *Nat. Phys.* **8**, 751-756 (2012).
- [19] G. Grissonnanche G, et al. Direct measurement of the upper critical field in cuprate superconductors. *Nat. Commun.* **5**, 1-8 (2014).
- [20] B. Vignolle, et al. Quantum oscillations and the Fermi surface of high-temperature cuprate superconductors. *C. R. Phys.* **12**, 446 (2011)
- [21] S. Sebastian, et al. Quantum oscillations in the high- T_c cuprates. *Phil. Trans. R. Soc. A* **369**, 1687 (2011)
- [22] A. V. Herzog, P. Xiong, R. C. Dynes. Magnetoresistance oscillations in granular Sn wires near the superconductor-insulator transition. *Phys. Rev. B*, **58**, 14199 (1998).
- [23] A. Johansson, G. Sambandamurthy, D. Shahar, N. Jacobson, R. Tenne, Nanowire Acting as a Superconducting Quantum Interference Device. *Phys. Rev. Lett*, **95**, 116805 (2005).
- [24] U. Patel, et al. Synthesis and superconducting properties of niobium nitride nanowires and nanoribbons, *Appl. Phys. Lett.* **91**, 162508 (2007).
- [25] J. Wang, et al. Magnetoresistance Oscillations of Ultrathin Pb Bridges. *Nano Res.* **2**, 671 (2009).
- [26] G. R. Berdiyrov, et al. Magnetoresistance oscillations in superconducting strips: A Ginzburg-Landau study. *Phys. Rev. B* **86**, 224504 (2012).
- [27] Milind N. Kunchur, Charles L. Dean, Boris I. Ivlev, Anomalous oscillatory magnetoresistance in superconductors. *Phys. Rev. B*, **94**, 054504 (2016).
- [28] Y. Wang, L. Li, N. P. Ong, Nernst effect in high- T_c superconductors. *Phys. Rev. B*, **73**, 024510 (2006).
- [29] G. Blatter, M. V. Feigel'man, V. B. Geshkenbein, A. I. Larkin, V. M. Vinokur, Vortices in high-temperature superconductors. *Rev. Mod. Phys.* **66**, 1125 (1994).
- [30] P. Gandit, J. Chaussy, B. Pannetier, R. Rammal, Magnetic properties of a superconducting network, *Physica B*, **152**, 32 (1988).
- [31] X. Zhao, et al. Correlation between T_c and n_s/m^* in $\text{Bi}_2\text{Sr}_2\text{CaCu}_2\text{O}_{8+\delta}$ single crystals. *Physica C*, **307**, 265-270 (1998).
- [32] M. Weber, et al. Magnetic-flux distribution and the magnetic penetration depth in superconducting polycrystalline $\text{Bi}_2\text{Sr}_2\text{Ca}_{1-x}\text{Y}_x\text{Cu}_2\text{O}_{8+\delta}$ and $\text{Bi}_{2-x}\text{Pb}_x\text{Sr}_2\text{CaCu}_2\text{O}_{8+\delta}$. *Phys. Rev. B*. **48**, 13022 (1993).

[33] B. Burk, R. E. Thomson, A. Zettl, and J. Clarke, Charge-density-wave domains in 1T-TaS₂ observed by satellite structure in scanning-tunneling -microscopy images. *Phys. Rev. Lett.* **66**, 3040 (1991).

[34] I. Vinograd, et al. Locally commensurate charge-density wave with three-unit-cell periodicity in YBa₂Cu₃O_y. *Nat. Commun.* **12**, 3274 (2021).

Supplementary information to:

Little-Parks like oscillations in lightly doped cuprate superconductors

Menghan Liao¹, Yuying Zhu², Shuxu Hu¹, Ruidan Zhong³, John Schneeloch^{3,4}, Genda Gu³, Ding Zhang^{1,2,5,6*}, and Qi-Kun Xue^{1,2,5,7*}

¹ *State Key Laboratory of Low Dimensional Quantum Physics and Department of Physics, Tsinghua University, Beijing 100084, China*

² *Beijing Academy of Quantum Information Sciences, Beijing 100193, China*

³ *Condensed Matter Physics and Materials Science Department, Brookhaven National Laboratory, Upton, New York 11973, USA*

⁴ *Department of Physics and Astronomy, Stony Brook University, Stony Brook, New York 11794, USA*

⁵ *Frontier Science Center for Quantum Information, Beijing 100084, China*

⁶ *RIKEN Center for Emergent Matter Science (CEMS), Wako, Saitama 351-0198, Japan*

⁷ *Southern University of Science and Technology, Shenzhen 518055, China*

*Corresponding author.

Email: dingzhang@mail.tsinghua.edu.cn, qkxue@mail.tsinghua.edu.cn

Contents

1. Estimation of B_{c2} and ξ_0 in under-doped Bi-2212
2. Resistance oscillations in under-doped Bi-2212 on SiO₂/Si substrates
3. Resistance oscillations in a Bi-2212 microbridge
4. Exclusion of extrinsic mechanisms for the low field resistance oscillations
5. Subtraction of the smoothed background
6. Doping dependence of the extracted fitting parameters

1. Estimation of B_{c2} and ξ_0 in under-doped Bi-2212

The measurement of B_{c2} in cuprate superconductors is not as straightforward as low-temperature superconductors. Not only B_{c2} often exceeds the highest available magnetic field, but also there exists complications brought by the vortex solid and liquid phases [16-18]. Previous studies often rely on measuring the Nernst effect instead of simple resistance measurements to determine B_{c2} . However, measurements of B_{c2} in the extremely underdoped regime ($p \leq 0.1$) remain scarce.

Based on our transport data, we obtain the magnetic field at which the vortex solid melts— B_{vs} at different temperatures below T_{c0} . Although $B_{vs}(T)$ is usually lower than the upper critical field $B_{c2}(T)$ at finite temperatures, previous experiments on a variety of cuprate superconductors (underdoped YBCO, overdoped Tl-Bi2201 [17,18], $\text{Nd}_{2-x}\text{Ce}_x\text{CuO}_4$ [16]) showed that $B_{vs}(T)$ becomes very close or even merges with $B_{c2}(T)$ at $T \rightarrow 0$ K. We therefore extrapolate B_{vs} down to 0 K to derive a lower limit of B_{c2} . Based

on $B_{c2}(0)$, one can readily calculate the values of ξ_0 by using the formula: $\xi_0 = \sqrt{\frac{\Phi_0}{2\pi B_{c2}}}$.

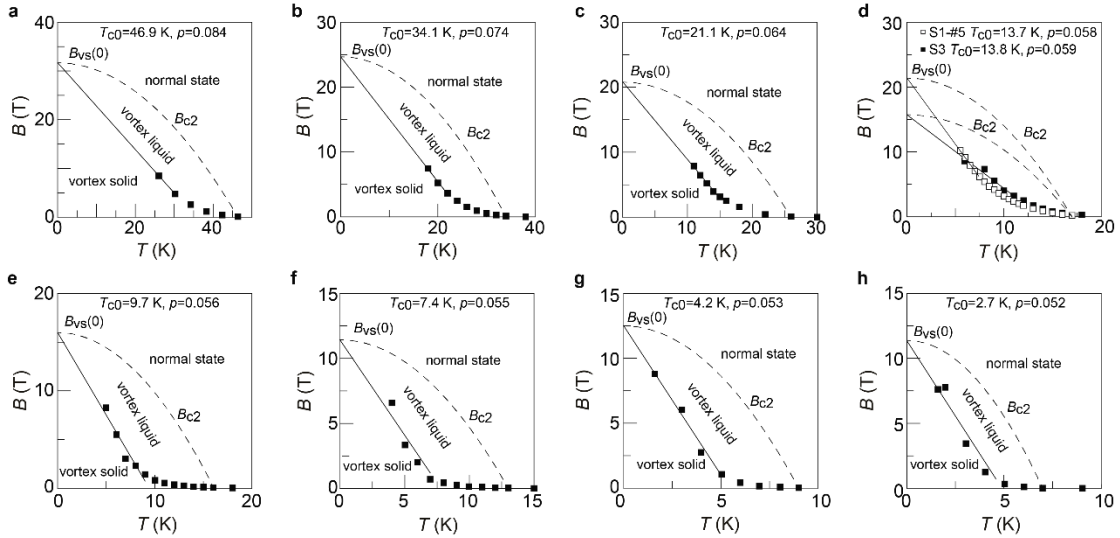


Fig. S1 Magnetic-field and temperature phase diagrams of underdoped Bi-2212. Data points indicate B_{vs} at a set of fixed T . They mark the magnetic field at which the magneto-resistance reaches 10% of the zero-field resistance value at 87 K. Filled symbols are for sample S3 at different doping levels. Empty symbols in **d** are extracted from sample S1 at the fifth gated stage. Solid lines are the linear extrapolations based on the data points at low temperatures. Dashed curves are a guide to the eye, showing the expected temperature evolution of the upper critical field B_{c2} [19].

Fig. S1 shows the temperature dependence of B_{vs} for two samples discussed in the main text and at different doping levels. Here we define B_{vs} as the field where the magneto-resistance reaches 10% of the normal state resistance (zero-field resistance at

87 K). Although a theoretical formula describing $B_{vs}(T)$ can be employed for fitting the data at finite temperatures [18], we find that this fitting gives rise to a large uncertainty of $B_{vs}(T \rightarrow 0)$ at small p . This uncertainty is mainly caused by the limited portion of the temperature window below T_{c0} that can be covered experimentally. Instead, we carry out a simpler evaluation by linearly extrapolating the data points to absolute zero (Solid lines in Fig. S1). The extrapolated values of $B_{vs}(0)$ are then taken as equal to $B_{c2}(0)$.

In Fig. S2, we plot the estimated $B_{c2}(0)$ as well as the calculated ξ_0 as a function of the doping level. The decreasing trend of B_{c2} as p decreases can also be inferred from the reduced B_{vs} at lower p in Fig. S1. Previous studies only measured Bi-2212 at $p \geq 0.1$ such that a direct comparison to our estimated ξ_0 at $p < 0.1$ is not possible. Nevertheless, we include in Fig. S1 the reported B_{c2} and ξ_0 values for YBCO at $p < 0.1$. They show consistent values and doping dependence as those of our estimated values in Bi-2212.

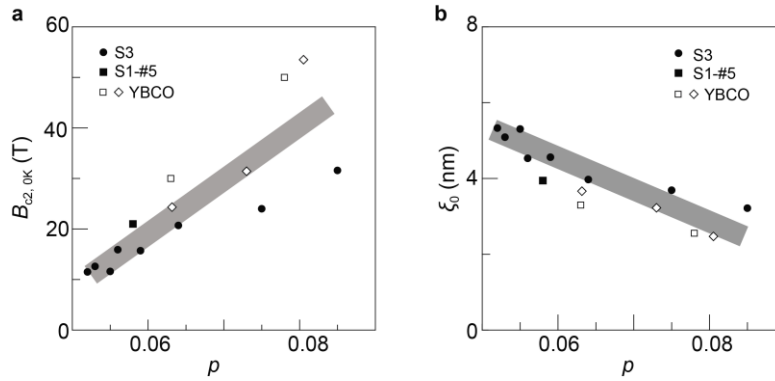


Fig. S2 Estimated B_{c2} and ξ_0 in underdoped Bi-2212. **a**, Filled symbols show the doping dependence of B_{c2} of underdoped Bi-2212 obtained from the linear extrapolations in Fig. S1. Empty diamonds and squares are the B_{c2} values of YBCO from ref. [17] and [18], respectively. **b**, Calculated ξ_0 of Bi-2212 and YBCO based on the corresponding B_{c2} in panel **a**.

2. Resistance oscillations in under-doped Bi-2212 on SiO₂/Si substrates

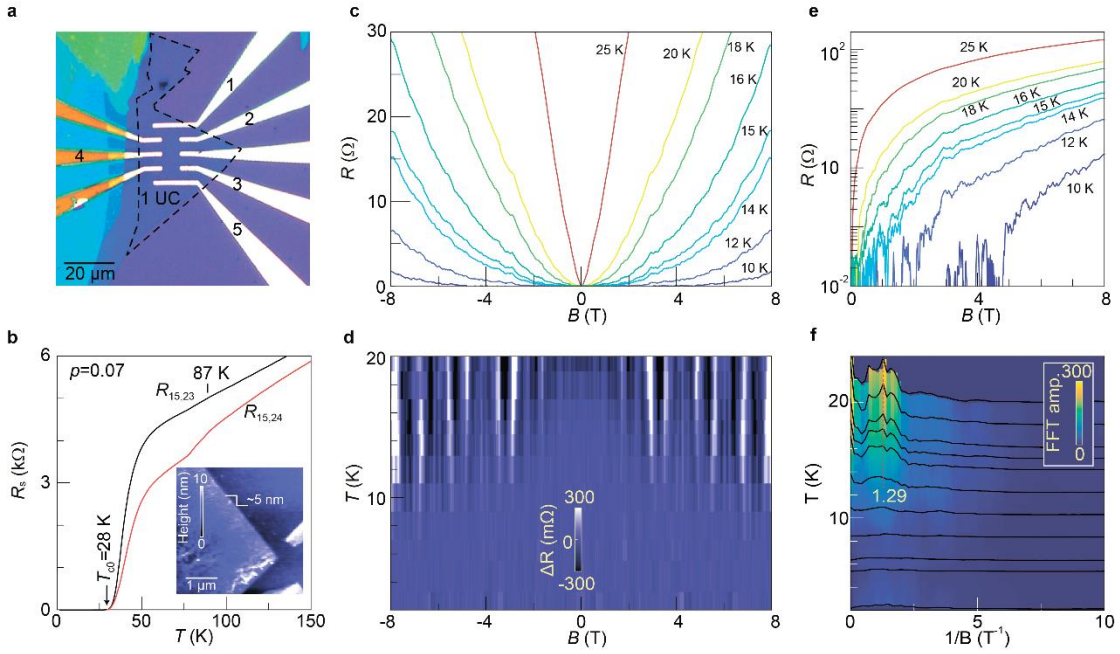


Fig. S3 Magneto-transport results of an ultrathin Bi-2212 flake (1 UC) on the SiO₂/Si substrate.

a, Optical image of sample S5. The dashed line demarcates the 1 UC region. Specific contacts used in transport are marked with numbers. **b**, Sheet resistance of S5 as a function of temperature. Red (Black) curve is obtained by passing the current from contact 1 to contact 5, as indicated in **a**, and measuring the voltage between contacts 2 and 4 (2 and 3). The kink at around 87 K is presumably from the thicker flakes contacted by electrode-4 (see panel **a**), which remain in the initial doping regime. Inset shows the AFM image of S5 after the transport measurements. The step height is about 5 nm. **c**, Resistance of S5 as a function of magnetic field at a set of temperature points. **d**, Color plot of the background subtracted resistance of S5. **e**, Same magneto-resistance traces as in **C** but plotted with the y-axis in log scale to enhance the oscillatory features. **f**, FFT of the background subtracted resistance traces at different temperatures. Vertical dotted line with the number marks the peak positions.

We observe similar resistance oscillations in exfoliated Bi-2212 flakes on SiO₂/Si substrates. These samples are not intercalated by lithium ions. They are driven into the under-doped regime by varying the oxygen content directly. Figure S3 shows the data of one such sample—S5. The thickness is about 1 UC, as can be roughly determined by the optical contrast (Fig. S3a). The sample was further capped by a thin flake of hexagonal boron nitride (hBN) for protection against air exposure.

Fig. S3b shows the temperature dependent resistance of S5. The resistance values are similar to that reported previously in 1 UC Bi-2212 [35], reaffirming the ultrathin nature of our flake. Clearly, S5 possesses a T_c of 28 K, indicating that it is in the underdoped regime. The reduction of doping is caused by natural oxygen loss during the

sample processing in the glovebox. Similar loss of oxygen for the ultrathin Bi-2212 flake was reported before [36].

Fig. S3c illustrates the magneto-resistance at different temperatures. Oscillatory features start to appear symmetrically around $B = 0$ T below 25 K. In Fig. S3d, we show the color-coded data with the smoothed background subtracted. Prominent zebra stripes occur around the superconducting transition region. In Fig. S3e, the magneto-resistance is shown in a logarithmic scale. Both plots (panels d and e) show repeatable oscillations at various temperatures. Furthermore, the FFT of the background subtracted traces (Fig. S3f) gives rise to a peak at around 1.29 T^{-1} , corresponding to ΔB of about 0.78 T. This period is similar to that obtained in lithium intercalated Bi-2212.

After the transport measurements, we peeled off the hBN layer and measured the sample thickness by atomic force microscopy (AFM). The AFM image is shown as an inset of Fig. S3b. The step height at the edge of the sample is about 5 nm. This apparent thickness of the Bi-2212 flake is thicker than the nominal value of 3 nm for 1 UC flake. As found previously, the thickness determined by AFM is usually larger than the theoretical values, presumably due to the different chemical potentials of Bi-2212 and SiO_2 [35].

A second Bi-2212 flake on SiO_2/Si , which shows low-field oscillations, is presented in the next section.

3. Resistance oscillations in a Bi-2212 microbridge

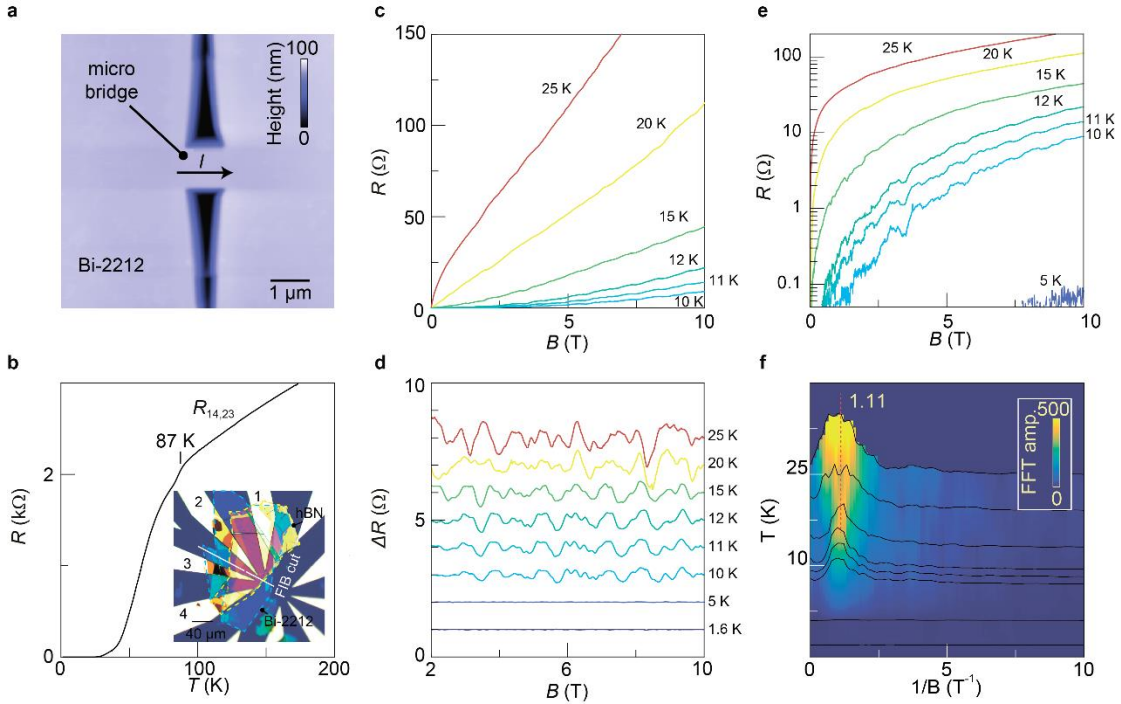


Fig. S4 Resistance oscillations of a Bi-2212 micro-bridge. **a**, AFM image of the Bi-2212 micro-bridge. **b**, Temperature dependent resistance of the sample. The kink at 87 K can be attributed to the region farther from the micro-bridge, which remains the initial doping level. Inset shows an optical image of the device. The central part of the Bi-2212 flake (marked by blue dashed lines) is covered by h-BN (yellow dashed line) for protection. White straight line indicates the cutting direction for the focused ion beam (FIB). The resistance is measured by passing the current from contact 1 to 4 and measuring the voltage between contacts 2 and 3. **c**, Magneto-resistance traces at a set of temperatures. **d**, Background subtracted magneto-resistance at different temperatures. **e**, Same magneto-resistance traces as in **c** but plotted with the y-axis in log scale to enhance the oscillatory features. **f**, FFT of the background subtracted resistance traces at different temperatures. Vertical dotted line with the number marks the peak positions.

To investigate the mesoscopic effect as a possible cause for the low-field oscillations, we intentionally pattern a microbridge in Bi-2212 flake. Figure S4a and inset of Fig. S4b display our sample. The Bi-2212 flake is about 20 nm thick (~ 6 UC) and is capped by hBN for protection. A microbridge with a width of $1 \mu\text{m}$ was patterned by using focused ion beam (FIB) with Ga^+ ions at 15 kV. The FIB cutting direction is schematically shown in the optical image in the inset of Fig. S4b.

Fig. S4b shows the temperature dependent resistance, indicating that $T_{c0} = 25$ K. It suggests that the sample is in the underdoped regime with $p = 0.067$. Again, the flake was exfoliated from the nearly optimal doped bulk crystal. It became underdoped presumably due to the oxygen loss during the FIB process.

Fig. S4c-e show the magneto-resistance traces and the background subtracted ones. The oscillation amplitude is comparable to those observed in flakes without patterning the micro-bridge. Furthermore, the FFT in Fig. S4f shows a peak at 1.11 T^{-1} , which is consistent with the values obtained from other samples. These results suggest that the low-field oscillations show no apparent dependence on the channel width in the range from $1 \mu\text{m}$ to $80 \mu\text{m}$. The mesoscopic effect seems to play a negligible role in giving rise to the oscillations.

4. Exclusion of extrinsic mechanisms for the low field resistance oscillations

Fig. S5 shows the resistance curves obtained at the same temperature but with different field-sweep directions or sweep rates. We also measured the resistance with different currents. All of the curves show oscillating features at the same magnetic field. External perturbation such as electrical noise, flux jump in the superconducting magnet, temperature instability etc. can be therefore excluded as the reason for the oscillations.

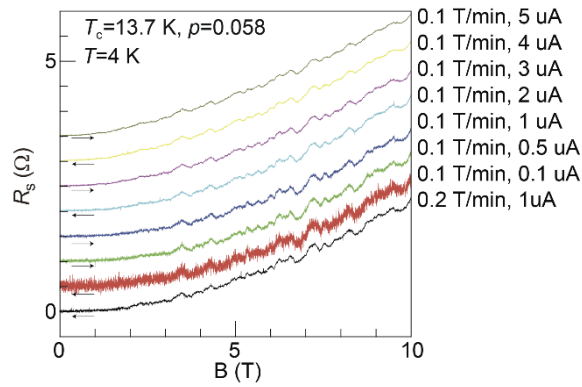


Fig. S5 Magneto-resistance of sample S2. Curves are obtained with different excitation currents, different sweep rates and directions of magnetic field. The sweep directions are marked by the black arrows.

5. Subtraction of the smoothed background

To obtain the data shown in Figs. 1d, 2b, S3d and S4d, we subtract the original magneto-resistance by smoothed backgrounds. To obtain the smoothed backgrounds, we take the following steps. First, we interpolate the measured data such that the magnetic field spacing is 1 mT, i.e. 1000 points/T. Then, we run a moving average over 1000 data points to obtain the background curve. In Fig. S6, we compare the data obtained by subtracting such a background to that from a different method. In Fig. S6a, the subtracted background is still the moving averaged one. To obtain the data shown in Fig. S6b, we subtract a background that is a polynomial fitting to the original magneto-resistance (to the seventh order). The right panels of Fig. S6 compare the FFT results of the data obtained by the two methods. In general, they show qualitatively no difference and the oscillation periods obtained are the same.

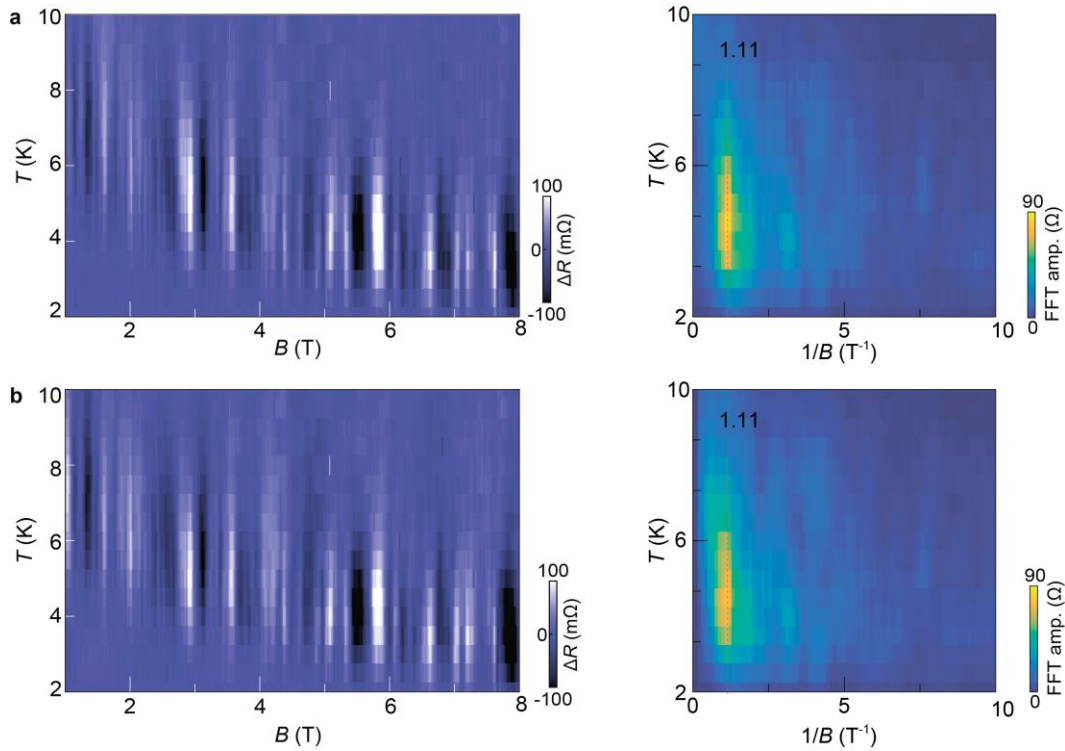


Fig. S6. Comparison of the resistance oscillations obtained by two different background subtraction methods. **a**, (Left) ΔR as a function of magnetic field and temperature. (Right) FFT of $\Delta R(B)$ at different T . Here, the subtracted background is obtained by smoothing the original curve in a range of 1 T (running average). **b**, ΔR and its FFT of the same data set of magneto-resistance. However, ΔR is obtained by subtracting a polynomial fit to the original curve.

6. Doping dependence of the extracted fitting parameter

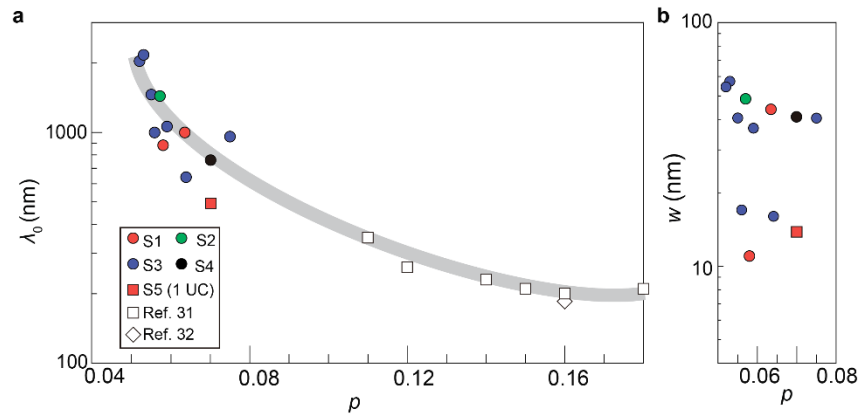


Fig. S7 Doping dependence of the extracted fitting parameter λ_0 and w . Filled symbols in A and B are the data points from our fitting. Empty squares in A are measured penetration depth in Bi-2212 [31]. Empty diamond in A is the reported value for Bi-2212 in ref. [32].

p	ξ_0 (nm)	a (nm)	T_c (K)	R_n (Ω)	w (nm)	λ (nm)
0.075	3.68	42.1	35	0.14	40.8	960
0.064	3.97	52.4	30	0.71	16	640
0.059	4.56	38.5	21	0.63	37	1060
0.056	4.53	45.5	20	2.5	17	1000
0.055	5.3	42.2	18	1.42	41	1460
0.053	5.1	57.0	15	4.83	57	2220
0.052	5.3	54.4	15	4	54	2040

Table S1 Summary of parameters for sample S3 at different doping levels. Here the doping level p is evaluated by using the experimentally measured T_{c0} and the formula: $T_{c0} = T_{c,max}[1 - 82.6(p - 0.16)^2]$. The coherence length ξ_0 is estimated from the magneto-transport data, as explained in supplementary information, section 1. a is the period extracted from the resistance oscillations. The rest of the parameters: T_c (critical temperature), R_n (normal state resistance), w (separation of the non-superconducting region in the superconducting mesh, as illustrated in Fig. 5) and λ (penetration depth) are used in Eq. (1). In addition, the superconducting thickness in Eq. (1) is chosen to be: $d = 1.5$ nm, which is the thickness of half of a unit cell of Bi-2212. We choose this value because Bi-2212 is a layered superconductor with strong anisotropy and weak interlayer coupling.

References

- [35] D. Jiang, et al. High- T_c superconductivity in ultrathin $\text{Bi}_2\text{Sr}_2\text{CaCu}_2\text{O}_{8+x}$ down to half-unit-cell thickness by protection with graphene. *Nat. Commun.* **5**, 1-8 (2014).
- [36] Y. Yu, et al. High-temperature superconductivity in monolayer $\text{Bi}_2\text{Sr}_2\text{CaCu}_2\text{O}_{8+\delta}$ *Nature*, **575**, 156-163 (2019).